The Astronomical Journal, 133:2327–2333, 2007 May

PHOTOMETRY AND KINEMATICS OF TWO MINOR MERGER CANDIDATE GALAXIES

Germán N. Gimeno,[1,2] Horacio A. Dottori,[3] Rubén J. Díaz,[4,5]
Irapuan Rodrigues,[3] and Gustavo J. Carranza[6]
Received 2006 October 18; accepted 2007 January 13

ABSTRACT

We observationally investigate the properties of disk galaxies undergoing minor merger or capture events. In this context, the properties of two double-nucleus candidate galaxies, ESO 381–IG 23 and MCG −3-35-14, are analyzed. Both are disk-dominated Sc–Scd galaxies that show a bright knot superposed on their disk body. The size and surface brightness of these knots are in both cases comparable to those of the galaxy nucleus, which has led previous work to classify these galaxies as double-nucleus galaxies. We present results from observations made with the SOAR 4.1 m, CASLEO 2.15 m, and Bosque Alegre 1.54 m telescopes. We determined the values for the apparent and absolute magnitudes of the nuclei and the bright regions and analyzed the surface brightness profiles and colors. We also study the kinematics of the galaxies via their rotation curves. Analytical mass models were fitted under the constraints of both kinematic and photometric observational data. It is found that ESO 381–IG 23 has an absolute magnitude $M_B = -19.59$ and mass $\mathcal{M} = (3.0 \pm 0.2) \times 10^{10}\ \mathcal{M}_\odot$, and its nuclear spectrum shows strong emission lines typical of starbursts. MCG −3-35-14 has $M_B = -19.97$ and $\mathcal{M} = (9.6 \pm 0.5) \times 10^{10}\ \mathcal{M}_\odot$. Both galaxies are morphologically normal disk galaxies. They have a bulge-to-disk ratio of ∼0.1 and show no significant signatures of dynamical perturbation in their rotation curves. The secondary nuclei candidates are found to be giant H II regions, rather than nuclei of captured companions. They have masses of $(2.2 \pm 0.2) \times 10^6\ \mathcal{M}_\odot$ (ESO 381–IG 23) and $(4.1 \pm 0.2) \times 10^6\ \mathcal{M}_\odot$ (MCG −3-35-14), and ages of 6.6 ± 0.1 and 8.0 ± 1.0 Myr, respectively.

Key words: galaxies: kinematics and dynamics — galaxies: nuclei — galaxies: spiral — galaxies: structure

Online material: color figure

1. INTRODUCTION

As part of an observational program of disk galaxies with double-nucleus and evolved minor merger candidates, detailed analysis of the morphology and kinematics of such systems is being carried out (Gimeno et al. 1998, 1999, 2000, 2005b), after an initial statistical investigation (Gimeno et al. 2004, hereafter Paper I). One of the aims of the present study is to determine whether these objects are truly double-nucleus entities. This is a key point, since we want to investigate systems originating from the interaction of a disk galaxy with satellite galaxies or simply smaller companions. For example, in some previous works, many Markarian double-nucleus galaxies (e.g., Mazzarella & Boroson 1993 and references therein) turned out to be normal galaxies, with the secondary nucleus being a giant H II region, hardly distinguishable from a nucleus on the photographic plates (e.g., Joseph et al. 1988). In other cases the situation was even worse: the secondary nucleus was no more than a superposed foreground star. Nevertheless, in many cases the secondary is indeed a nucleus of a merging or captured companion. As we seek secondary nuclei superposed on the disk, i.e., relatively close, the merger stage should be more or less advanced. The investigation of the state of disruption of the secondary is another major goal. The accretion of stripped material significantly affects the dynamical evolution of the primary galaxy. In particular, the origin of thick disks is ligated to this process (e.g., Ibata 2002).

Many of the objects deserve attention of their own. In this work the two galaxies investigated are examples of late-type disk-dominated galaxies. The importance of obtaining optical kinematical data of this type of galaxy has been stressed in relation to the overall distribution of matter and the dark matter fraction (e.g., Matthews & Gallagher 2002, hereafter MG02). In addition, since disk-dominated galaxies are mostly unevolved systems, those undergoing a capture event are a particularly interesting scenario in which to investigate the impact of the interaction on the disk structure and kinematics (e.g., Díaz et al. 2000, 2006).

We have observed the galaxies ESO 381–IG 23 and MCG −3-35-14 with high-resolution optical spectroscopy combined with surface photometry and optical color analysis. We also constructed analytical models of the mass distribution to fit the kinematical data. These models may be used as an initial condition to investigate the putative satellite orbits.

The paper is organized as follows: § 2 describes the observations and data reduction procedures, §§ 3 and 4 are devoted to the individual objects and § 5 to the H II regions, and § 6 contains the discussion and § 7 the final remarks.

2. OBSERVATIONS AND DATA REDUCTION

We obtained *B*, *V*, *R*, and *I* images with the 4.1 m SOAR telescope in the early science phase, in queue mode, during 2005 June and July. The instrument used was the SOI (Soar Optical Imager). It is a bent-Cassegrain mounted optical imager using

[1] Visiting Astronomer, Complejo Astronómico El Leoncito, operated under agreement between the Consejo Nacional de Investigaciones Científicas y Técnicas de la República Argentina and the National Universities of La Plata, Córdoba, and San Juan.
[2] Observatorio Astronómico de Córdoba, Córdoba; and Consejo Nacional de Investigaciones Científicas y Técnicas (CONICET), Argentina.
[3] Instituto de Física, Universidade Federal do Rio Grande do Sul, Porto Alegre, Brazil.
[4] Gemini Observatory, Southern Operations Center, c/o AURA, La Serena, Chile.
[5] Complejo Astronómico El Leoncito, CONICET, Argentina.
[6] Facultad de Matemática, Astronomía, y Física, Universidad Nacional de Córdoba, Córdoba; and CONICET, Argentina.

two EEV 2050×4100 CCDs to cover a $5.26'$ field of view at a scale of $0.077''$ pixel^{-1}. The full image has a gap of $10.8''$ between the two CCDs. A 2×2 binning results in a pixel size of $0.154''$. The seeing in the R band was better than $0.8''$. The images were flat-fielded, bias-subtracted, trimmed, and mosaicked by the SOAR staff members.

Surface brightness profiles along the major axis were extracted from the SOAR images. The main advantage of taking the major-axis profile is that it enables us to better analyze the surface brightness behavior in the inner regions, and uncertainties due to projected internal extinction are minimized. On the other hand, azimuthally averaging the profile minimizes the bumps present in major-axis profiles due to spiral arms and dust-lane absorptions. We have used both as constraints for the purpose of fitting calculated profiles.

Surface brightness radial profiles were constructed by plotting the pixel surface brightness,

$$\mathrm{SB} = m + 2.5 \log A - 2.5 \log\left(\frac{f_{\mathrm{pix}}}{f}\right), \tag{1}$$

versus deprojected galactocentric distance, along the primary galaxy major axis, as well as along several other position angles (m is the galaxy magnitude, $A = 0.154^2$ is the pixel area in square arcseconds, and f_{pix} and f are the pixel and galaxy fluxes, respectively). The magnitudes and colors of the nuclei and the H II regions were determined with the SOAR images, within a $3''$ diameter aperture.

Images were also taken with the Multifunctional Integral Field Spectrograph (MIFS) in direct imaging mode (for a description of the instrument, see Díaz et al. 1999 and references therein) at the Bosque Alegre (BA) 1.54 m telescope in Córdoba, Argentina, with a scale of $0.76''$ pixel^{-1}, from which the total $BVRI$ magnitudes of both galaxies were determined.

Long-slit spectra were obtained with the REOSC spectrograph coupled to the 2.15 m telescope at the CASLEO, San Juan, Argentina, between 2005 October and 2006 March. A 1200 line mm^{-1} grating was used in order 1 with a scale of 0.6 Å pixel^{-1} in the Hα region. The slit was 300 μm wide with an effective spectral resolution of 2 Å. The spatial scale was $1''$ pixel^{-1}. The slit was oriented along the apparent major axis. The overall exposure times were 120 minutes for ESO 381–IG 23 and 90 minutes for MCG −3-35-14, achieving a mean signal-to-noise ratio (S/N) in Hα of better than 20 and 10, respectively.

Long-slit spectra were also obtained for ESO 381–IG 23 with the MIFS in the long-slit mode at the BA 1.54 m telescope in 2000 February, with a 1200 line mm^{-1} grating and a scale of 0.8 Å pixel^{-1} in the Hα region. The slit was 250 μm wide with an effective spectral resolution of 2 Å. The spatial scale was $1.52''$ pixel^{-1}. The overall exposure time was 90 minutes, and the slit was oriented along the two nuclei, revealing emission lines from both of them but much more intense in the secondary.

Data reduction was performed mainly with ADHOC software (Boulesteix 1993). Once reduced, the individual frames (spectra at the same position angle [P.A.] and images in the same filter) were co-added together in order to increase the S/N. Frame recentering was carried out with an accuracy of 0.1 pixels.

2.1. *Spectra Reductions*

Spectra extractions from the co-added bidimensional frames were performed in $1''$ wide slices, which were wavelength-calibrated by interactively fitting the Hα emission-line parameters with Gaussian profiles. A CuNeAr lamp was used for generating the comparison spectrum. Since radial velocities were measured from a single emission line, the uncertainty of each velocity value was obtained from the expression

$$e_{\mathrm{Gau}} = 0.8\left(\frac{c\,\sigma_{\mathrm{cont}}}{I\,d^{1/2}}\,\frac{\delta\lambda^{3/2}}{\lambda}\right) \tag{2}$$

(Díaz et al. 2000; Keel 1996), where σ_{cont} is the noise at a nearby continuum region and I is the line intensity (both in ADU); $\delta\lambda$ is the line's FWHM, d is the spectrum dispersion in angstroms per pixel, and c is the velocity of light. The instrumental width of night-sky emission lines was about 100 km s^{-1}. Night-sky lines were used to check the zero points of the wavelength calibrations.

The mean value of the radial velocity was adopted as the systemic heliocentric radial velocity. The latter was corrected for Galactic rotation and used to derive the distances under the assumption $H_0 = 75$ km s^{-1} Mpc^{-1}.

2.2. *Kinematics and Mass Distribution Models*

The inclination of the galaxies was computed as

$$\cos^2 i = 1.042(1 - b/a)^2 - 0.042 \tag{3}$$

(Holmberg 1958), where b/a is the photometric axis ratio measured on the SOAR images.

For the mass distribution, we adopted the superposition of a spherical potential (Dehnen 1993) and a flattened one (Satoh 1980):

$$\begin{aligned}\phi(R, z) &= \phi_1(R, z) + \phi_2(R, z)\\ &= \frac{G\mathcal{M}_1}{2a_1}\left\{\frac{R^2 + z^2}{\left[(R^2 + z^2)^{1/2} + a_1\right]^2} - 1\right\}\\ &\quad - \frac{G\mathcal{M}_2}{\left\{R^2 + z^2 + a_2\left[a_2 + 2\left(z^2 + b_2^2\right)^{1/2}\right]\right\}^{1/2}},\end{aligned} \tag{4}$$

where $\mathcal{M}_1$ and a_1 are the spherical component mass and scale length, while $\mathcal{M}_2$, a_2, and b_2 are the same, except for the disk component; R and z are the cylindrical coordinates. The rotation curve on the meridional plane is

$$\begin{aligned}v_c(R) &= \sqrt{R\left.\frac{\partial\phi}{\partial R}\right|_{z=0}}\\ &= \left\{\frac{G\mathcal{M}_1 R^2}{(R + a_1)^3} + \frac{G\mathcal{M}_2 R^2}{[R^2 + a_2(a_2 + 2b_2)]^{3/2}}\right\}^{1/2},\end{aligned} \tag{5}$$

and the surface brightness profile is calculated from the mass density corresponding to the adopted potential; that is,

$$\mu = \sum_{i=1}^{2} \Upsilon_i^{-1} \int \rho_i\, dl, \tag{6}$$

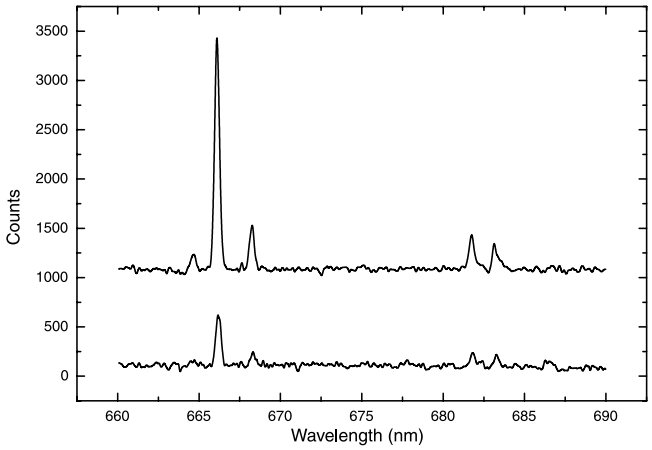

FIG. 1.—Long-slit spectra of ESO 323–IG 23 taken with the BA telescope: primary (*lower plot*) and secondary (*upper plot*) nucleus.

where

$$\rho_1 = \frac{\nabla^2\phi_1}{4\pi G} = \frac{3\mathcal{M}_1 a_1}{4\pi\left(\sqrt{R^2+z^2}+a_1\right)^4}, \tag{7}$$

$$\rho_2 = \frac{\nabla^2\phi_2}{4\pi G} = \frac{a_2 b_2^2 \mathcal{M}_2 R^2}{4\pi S^3\left(z^2+b_2^2\right)} \times\left[\frac{1}{\left(z^2+b_2^2\right)^{1/2}}+\frac{3}{a_2}\left(1-\frac{R^2+z^2}{S^2}\right)\right], \tag{8}$$

where $S^2 \equiv R^2 + z^2 + a_2[a_2 + 2(z^2 + b_2^2)^{1/2}]$ and $\Upsilon_i (i = 1, 2)$ is the mass-to-light ratio of the bulge and disk components, respectively. The first term of the integral (eq. [6]) has an analytic expression (Dehnen 1993), but the second term must be computed numerically.

Although in the present case the SOAR images have subarcsecond seeing, taking into account the effect of seeing to fit the inner regions is critical; not doing so may seriously bias some derived structural parameters such as characteristic scale lengths and central densities (Gimeno et al. 2005a; Schweizer 1979). Therefore, once the surface brightness was calculated, it was then convolved with the seeing PSF:

$$\mu^* = \mu \otimes f_{\rm PSF}. \tag{9}$$

This was then fitted to the observed profile. To derive the PSF, a Gaussian profile was fitted to the stellar sources on the galaxy image. Then,

$$\mu^*(X) = \frac{1}{\sqrt{2\pi}}\int \mu(X) e^{-(x-X)^2/2\sigma^2}\, dx, \tag{10}$$

where X is the apparent galactocentric radius and σ is the FWHM. The integrals in equations (6) and (10) were computed by means of specifically written FORTRAN programs and standard spreadsheets.

The value of Υ_i (assumed constant for each component) is determined as a result of the above procedure. The *I* profile was used, since it is more reliable as a tracer of the mass distribution given its lower sensitivity to internal extinction, and it is also the least affected by seeing. As said above, we used both major-axis and azimuthally averaged profiles to perform the fit.

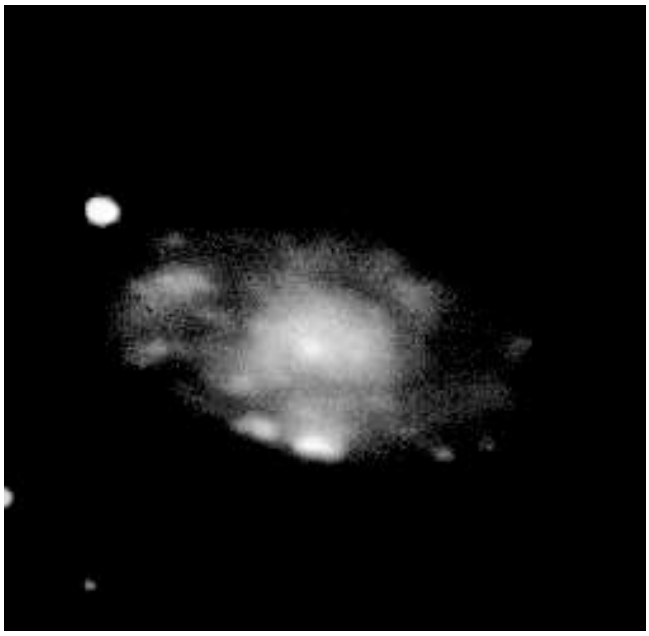

FIG. 2.—SOAR (SOI) *VRI* image of ESO 382–IG 23. The field size is $40'' \times 40''$. North is up, and east is to the left. The secondary nucleus candidate is $5''$ south of the main nucleus. [*See the electronic edition of the Journal for a color version of this figure*.]

3. ESO 381–IG 23

3.1. *Morphology and Photometry*

This is a small disk galaxy that was first classified as a double-nucleus galaxy in the ESO/Uppsala survey (Lauberts 1982) and was included in the catalog of Paper I. The major-axis apparent size is $40''$, corresponding to 11 kpc at a distance of 59 Mpc (for $H_0 = 75$ km s^{-1} Mpc^{-1}). The secondary nucleus candidate is a bright concentration $5''$ south of the disk center. Figure 1 shows the spectra extractions from both nuclei positions. The equivalent width of the Hα line is 50 Å in the secondary, suggesting that it could be a giant H II region, as in the case of Mrk 788 (Joseph et al. 1988).

High-resolution SOAR images allowed the confirmation of the last statement. Figure 2 shows the composite *VRI* image of ESO 381–IG 23 taken with the SOAR 4.1 m telescope during its early science phase. The "secondary nucleus" H II region (hereafter N2) is the brightest of many more. It can be seen that N2 is evidently elongated in the east-west direction; its approximate size is $1.5'' \times 0.75''$, corresponding to 400 pc $\times$ 200 pc. There is another region (hereafter N3) $1.5''$ to the west-northwest of N2, not noticeable on previous images, that is about half the size of N2. The true nucleus (N1) has a semistellar appearance, as can be seen on the *BVR* image shown in Figure 3. The entire galaxy, although having a fragmentary appearance, shows some hint of spiral structure and dust absorption lanes.

The results of the photometry are shown in Table 1. Both H II regions show similar color indices and are markedly bluer than those of the nucleus. They are also very bright indeed, with blue absolute magnitudes of -16.35 and -15.84, respectively. As already noted, N2 is brighter than the nucleus itself in the *B* band.

The radial profiles in the *B* and *I* bands are shown in Figure 4. There is a slight color gradient: the $B - I$ index decreases radially outward, with the youngest stellar populations lying on the periphery.

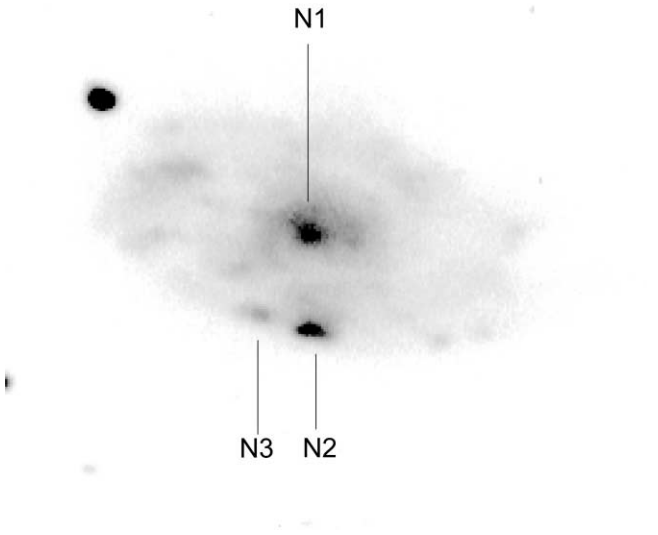

FIG. 3.—SOAR (SOI) *BVR* image of ESO 382–IG 23. The field size is 40″ × 40″. North is up, and east is to the left. The secondary nucleus candidate (N2) and the N3 region are shown. Note the elongated shape of N2 compared to the spherical main nucleus (N1).

3.2. *Kinematics and Mass Distribution*

The heliocentric radial velocity of the galaxy, derived from the center of symmetry of the radial velocity curve, is 4395 km s^{-1}. The observed and model rotation curves are shown in Figure 5. The observed curve is the average of both the receding and approaching side curves. It extends up to 5.2 kpc, the same as the photometric disk within 24.0 mag arcsec^{-2} in the *I* band. The rotation curve is typical of disks, rising shallowly and flattening at 130 km s^{-1} for $R \sim 3.5$ kpc. The parameters obtained for the fit of the model described in § 2.2 are shown in Table 2.

The intensity profile fit is shown in Figure 6, with the relative contributions of the bulge and the disk, and the total seeing-convolved, line-of-sight integrated intensity profile. The derived mass-to-light ratios are 1.0 for the bulge and 5.8 for the disk.

4. MCG −3-35-14

4.1. *Morphology and Photometry*

This is a spiral galaxy first cataloged by Vorontsov-Vel'yaminov & Arhipova (1968), with the description 2n; Da; Rf→1Sa, which stands for "two small nuclei; a smooth disk; and a faint large ring that becomes a long spiral arm." The galaxy has in fact a small nucleus and two well-developed spiral arms. A bright condensation—the secondary nucleus—lies on the western arm. It was included in Paper I as a double-nucleus galaxy candidate. The major axis's apparent size is 50″, corresponding to 25 kpc for a radial velocity of 7742 km s^{-1}, so it is more than twice the size of ESO 381–IG 23. Only *B*, *V*, and *R* images were obtained with SOAR. The *BVR* image is shown in Figure 7. The long, smooth spiral arms show a clear hint of asymmetry; the southwest arm is more tightly wound. The semistellar nucleus and the condensation have similar brightnesses, and there are also other bright knots in the spiral arms, clearly H II regions.

The results of the photometry are shown in Table 3. As in the previous case, the condensation shows bluer colors than the nucleus, and it is of comparable magnitude. It also has nearly the same absolute *B* magnitude as the giant H II (N2) region of ESO 381–IG 23, yet much less Hα emission. The inclination derived from equation (3) is 57°.

TABLE 1
PHOTOMETRY OF ESO 381–IG 23

Filter	Total	Nucleus[a]	H II (N2)[a]	H II (N3)[a]
B	14.25	17.51	17.49	18.00
B−*V*.....	0.57	0.56	0.22	0.22
V−*R*.....	0.39	0.53	0.34	0.40
R−*I*.....	0.15	0.28	−0.06	−0.18
M_B	−19.59	−16.33	−16.35	−15.84

[a] Within an aperture of radius 10 pixels, or ∼1.5″. The uncertainty in apparent magnitudes is 0.05, and 0.1 for color indices. All magnitudes and colors are corrected for Galactic extinction with values from Schlegel et al. (1998).

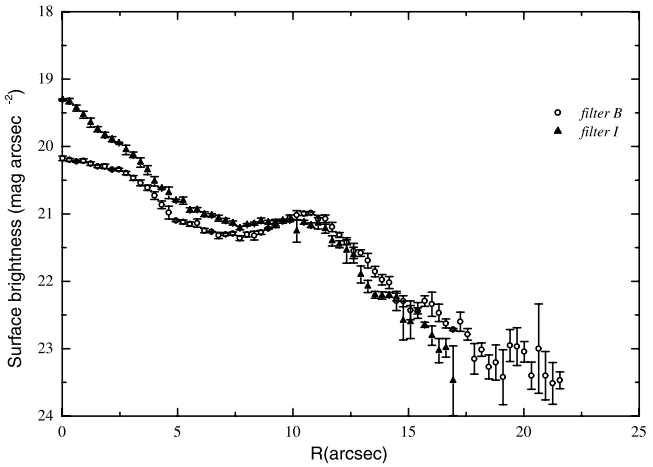

FIG. 4.—ESO 381–IG 23 *B* and *I* major-axis surface brightness profiles. The "bump" on the observed profiles between 8″ and 14″ is due to the lower mass-to-light ratio of the spiral arms; it smooths out if the azimuthally averaged profile is used instead of the major-axis profile.

4.2. *Kinematics and Mass Distribution*

The heliocentric radial velocity is 7742 km s^{-1}. The rotation curve is shown in Figure 8, together with the model curve. The shape of the rotation curve is similar to that of ESO 381–IG 23:

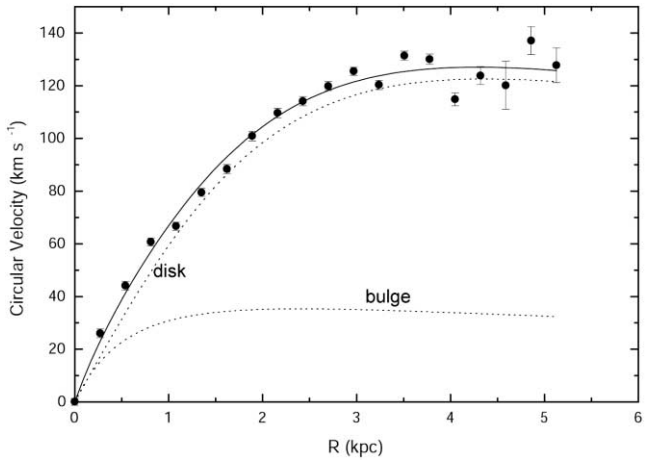

FIG. 5.—Rotation curve of ESO 381–IG 23: observed points (*circles*), model (*solid line*), and bulge and disk contributions (*dotted lines*). The angular separation between the observed data points is 1″.

TABLE 2
MASS MODEL PARAMETERS

Parameter	ESO 381–IG 23	MCG −3-35-14
$\mathcal{M}_1$ ($\mathcal{M}_\odot$)	0.023×10^{11}	0.06×10^{11}
a_1 (kpc)	1.2	1.2
Υ_1 ($\Upsilon_\odot$)	1.0	0.5
$\mathcal{M}_2$ ($\mathcal{M}_\odot$)	0.28×10^{11}	0.90×10^{11}
a_2 (kpc)	2.8	7.6
b_2 (kpc)	0.3	0.5
Υ_2 ($\Upsilon_\odot$)	5.8	1.1

it has a shallow rise and flattens at 140 km s^{-1}. The model (eq. [4]) was fitted again, and the resulting parameters are shown in Table 2. The bulge-to-disk ratio is 1/15; it is clearly also a disk-dominated system. The total resulting mass is 9.6×10^{10} $\mathcal{M}_\odot$, typical for a normal Sc galaxy.

The profile fit was performed in the same way as for ESO 381–IG 23, only this time the *R* band was used. The result is shown in Figure 9, where the observed major-axis profile is plotted together with that predicted by the model. The implied mass-to-light ratios are 0.5 for the bulge and 1.1 for the disk.

5. THE NATURE OF THE H II REGIONS

The physical parameters of the H II regions were estimated from evolutionary models from Starburst99 (Leitherer et al. 1999, hereafter L99).

5.1. *ESO 381–IG 23*

5.1.1. *The N2 Region*

As seen in Table 1, $M_B = -16.35$. This implies a mass value not smaller than 10^6 $\mathcal{M}_\odot$ (see Fig. 49 of L99; the mass is computed as described below). Next we consider the observed $B - V = 0.22$. For an instantaneous burst model with metallicity $z = 0.020$, this corresponds to an age between 6 and 8 Myr (see Fig. 57 of L99). Low metallicities can be ruled out, since the observed value of $B - V$ would imply 500 Myr (see Fig. 57 of L99) and mass values that are too high ($\sim 10^8$ $\mathcal{M}_\odot$), which is certainly not the case.

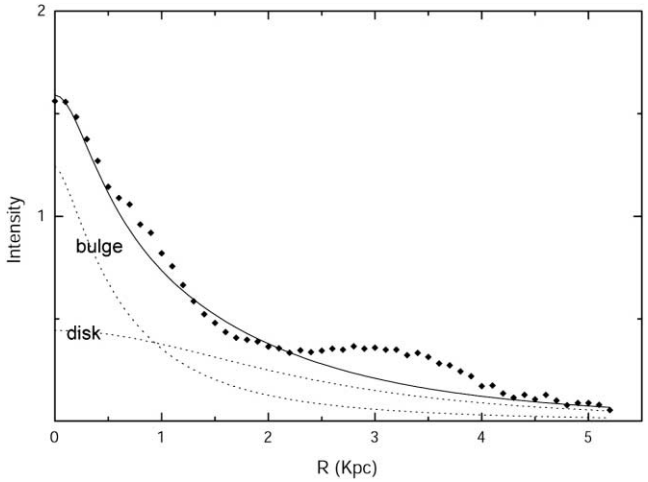

FIG. 6.—ESO 381–IG 23 *I* surface brightness profile (*diamonds*), model surface brightness (*solid line*), and bulge and disk contributions (*dotted lines*). The intensity scale is linear and in arbitrary units. The "bump" on the observed profile between 2.5 and 4 kpc is due to the lower mass-to-light ratio of the spiral arms; it smooths out if the azimuthally averaged profile is used instead of the major-axis profile. There is also some hint of circumnuclear star formation between 0.5 and 1 kpc.

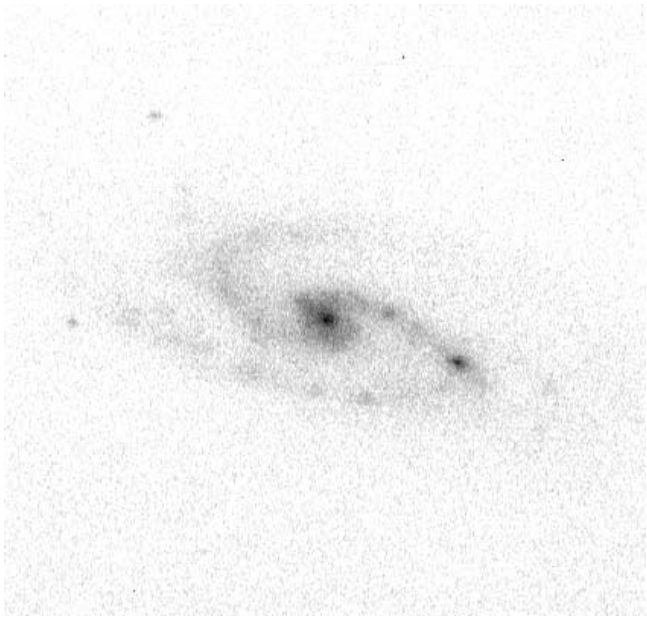

FIG. 7.—*BVR* image of MCG −3-35-14 obtained with the SOAR SOI. The field size is $65'' \times 65''$. North is up, and east is to the left. The secondary nucleus candidate lies on the western spiral arm turnover, $14''$ to the west-southwest of the main nucleus.

We then adopted the calculated model of L99, with $z = 0.020$, an instantaneous burst, $\alpha = 2.35$, and $\mathcal{M} = 100$ $\mathcal{M}_\odot$ up. The age was determined from this model, and the observed $V - I = 0.28$ (Fig. 10), yielding the result $t_{\rm burst} = 6.57 \pm 0.10$ Myr. The absolute magnitude for this age value is $(M_B)_{10^6\,\mathcal{M}_\odot} = -15.52$. Therefore, in order to reproduce the observed M_B, the mass value needed is $(2.2 \pm 0.2) \times 10^6$ $\mathcal{M}_\odot$ (the uncertainty comes from that on the absolute magnitude). With these values for the age and mass, the number of O stars for the adopted model is about 800 (see Fig. 37 of L99). And as said before, the size of N2 is approximately 400 pc × 200 pc (at a distance of 59 Mpc, $1''$ corresponds to 270 pc; the distance was determined as explained in § 2.1). Thus, N2 is among the greatest giant extragalactic H II regions (e.g., Dinerstein 1990; McCall et al. 1985).

5.1.1.1. The Physical Conditions in N2

The electronic density N_e was derived from the observed intensity ratio of the collisionally excited lines of [S II] $\lambda\lambda$6717–6731 from BA spectra, and the theoretical curve of $I(\lambda 6717)/I(\lambda 6731)$ versus $\log N_e$ (e.g., Stanghellini & Kaler 1989). Assuming $T_e = 10^4$ K, the value obtained is $N_e = 10^2$ cm^{-3}. We can estimate the radius $\mathcal{R}$ of the ideal Strömgren sphere from

$$nQ = (4/3)\pi \mathcal{R}^3 N_e^2 \alpha_B \qquad (11)$$

TABLE 3
PHOTOMETRY OF MCG −3-35-14

Filter	Total	Nucleus[a]	Condensation[a]
B	15.52	18.95	19.26
$B-V$	0.42	0.83	0.38
$V-R$	0.35	0.21	0.07
M_B	−19.97	−16.54	−16.24

[a] Within an aperture of radius 10 pixels, or $\sim 1.5''$. The uncertainty in apparent magnitudes is 0.05, and 0.1 for color indices. All magnitudes and colors are corrected for Galactic extinction with values from Schlegel et al. (1998).

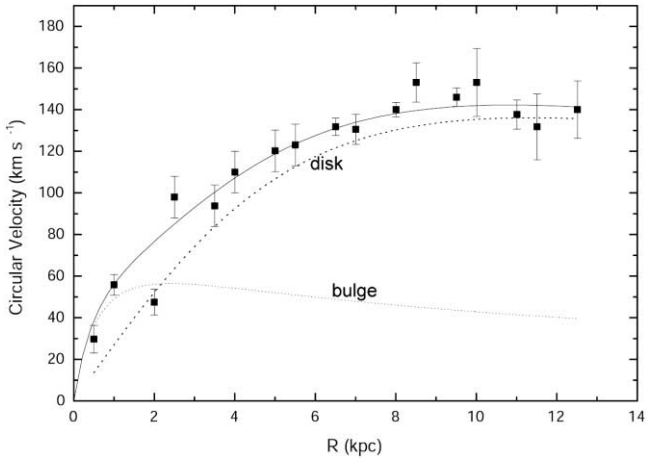

FIG. 8.—Rotation curve of MCG −3-35-12: observed points (*squares*), model (*solid line*), and bulge and disk contributions (*dotted lines*). The angular separation between observed data points is 1″.

under case B recombination, where n is the number of ionizing stars, Q is the number of ionizing photons per star, and α_B is the recombination rate to all levels except the ground state (we neglect diffuse radiation and make the pure hydrogen approximation for this calculation). Taking $Q = 5 \times 10^{49}$ (corresponding to an O star with $T = 10^4$ K), $\alpha_B = 8.7 \times 10^{-14}$ cm^3 s^{-1} (e.g., Osterbrock 1989), and $n = 800$, the result is $\mathcal{R} \approx 70$ pc. With the volume of the N2 region estimated by considering it an ellipsoid of axes 400 pc × 200 pc × 200 pc, the volume filling factor is 0.18.

5.1.2. *The N3 Region*

The same reasoning outlined for the N2 region applies to N3; both have similar colors, and the results are practically the same with regard to age and metallicity. The age determined by applying the same model and the observed $V - I = 0.22$ (Fig. 10) is $t_{\rm burst} = 6.50 \pm 0.10$ Myr. But, since $M_B = -15.84$, the resulting mass is $1.35 \times 10^6\ \mathcal{M}_\odot$. Thus, both regions have the same age and possibly are part of the same complex.

5.2. *MCG −3-35-14*

Unfortunately, there was no *I*-band image for this object; nevertheless, the age of the H II region can still be estimated from

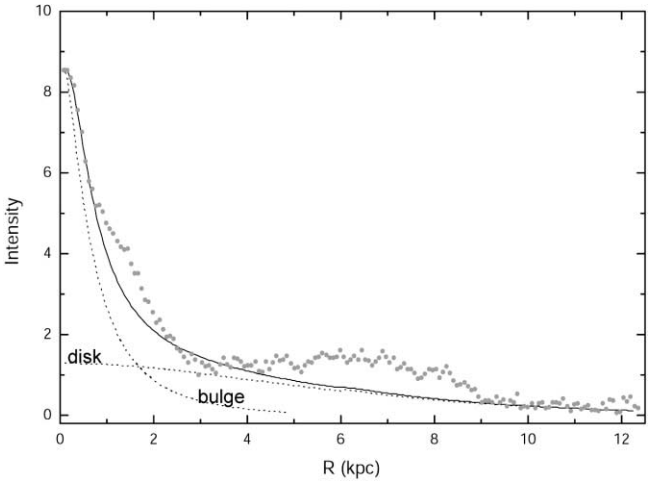

FIG. 9.—Same as Fig. 6, but for MCG −3-35-14. The "bump" on the observed profile between 4.2 and 9 kpc is due to the lower mass-to-light ratio of the spiral arms. There is also some hint of circumnuclear star formation between 1 and 2 kpc.

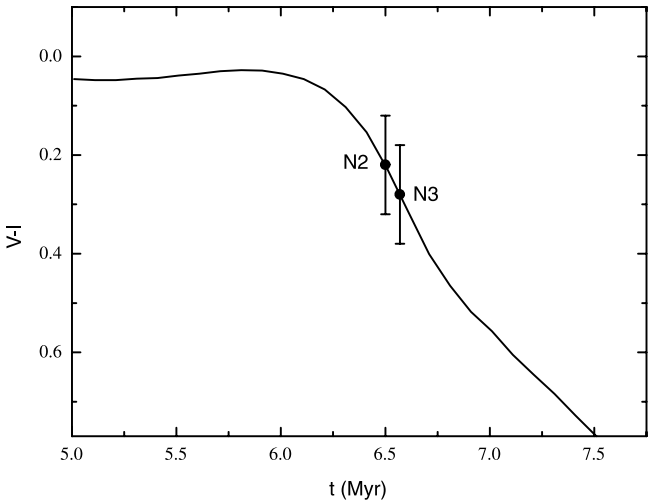

FIG. 10.—$V - I$ vs. t for the H II regions of ESO 381–IG 23. The curve is that of the adopted model of L99 ($z = 0.020$, instantaneous burst, $\alpha = 2.35$, and $\mathcal{M}_{\rm up} = 100\ \mathcal{M}_\odot$).

the $B - V$ color evolution (see Fig. 57 of L99), although here internal absorption effects may be stronger. With the same model adopted as for the previous regions, the result is $t_{\rm burst} = 8.0 \pm 1.0$ Myr. With this value for the age, the mass is $(4.1 \pm 0.2) \times 10^6\ \mathcal{M}_\odot$, nearly twice that of N2.

The number of ionizing photons with $\lambda < 912$ Å was calculated this time from Figure 77 of L99 for the derived age and mass. With this number ($10^{50.69}$ s^{-1}) and assuming $N_e = 10^2$ cm^{-3}, from equation (11) we have $\mathcal{R} \approx 26$ pc. The diameter of the region measured on the SOAR image is 1″, corresponding to 495 pc, so the filling factor is 1.2×10^{-3}.

6. DISCUSSION

The rotation curves have shallow velocity gradients, rising mildly from the center up to a circular velocity of 130 km s^{-1} (ESO 381–IG 23) and 140 km s^{-1} (MCG −3-35-14). This behavior is characteristic of late-type, disk-dominated Sc–Scd galaxies (e.g., MG02). The bulge contribution is not larger than 10%. The rotation curves are also symmetric and unperturbed, indicating that these galaxies have undergone an isolated evolution. Thus, the picture is consistent with ESO 381–IG 23 being a

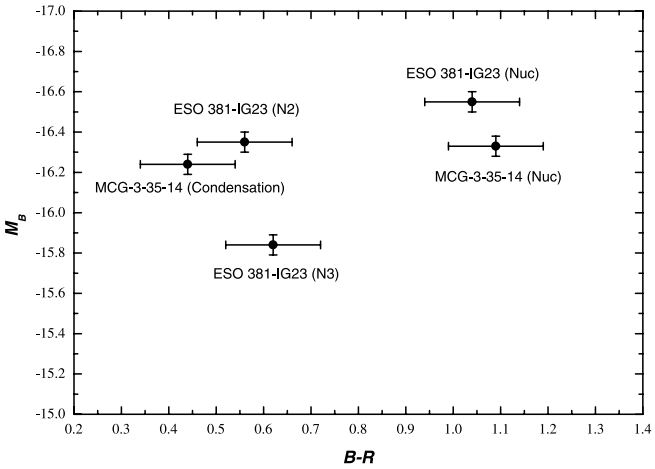

FIG. 11.—M_B vs. $B - R$ color-magnitude diagram for the nuclei and H II regions. The true nuclei are well separated from the H II regions.

small, young, star-forming Scd spiral and MCG −3-35-14 being a normal Sc spiral with a relatively quiet history. Nevertheless, a past minor interaction in the latter cannot be completely ruled out, given the slight asymmetry of the spiral arms (e.g., Zaritsky & Rix 1997) and a faint trail visible in the *BVR* image near the brightest H II region (also visible in the Palomar Observatory Sky Survey *B*-band image). Perhaps one would be tempted to associate this trail with an accreted satellite, with the bright condensation resulting from a starburst triggered by the interaction.

Figure 11 shows the M_B versus $B - R$ color-magnitude diagram for the nuclei and regions investigated. The true nuclei are well separated from the H II regions, with the latter ranging over a color interval only 0.2 mag wide. It has been shown that the three giant H II regions share similar properties, and their physical conditions make them comparable to other known regions, such as the "jumbo" region of NGC 3310 (e.g., Pastoriza et al. 1993). These authors modeled the burst of the jumbo region with a two-aged model (5 and 14.5 Myr) containing 570 O stars and 200 W-R stars (a total of 770 ionizing stars; compare to our 800 for N2).

7. CONCLUSIONS

Two disk-dominated galaxies were investigated with moderate-resolution spectroscopy and SOAR high spatial resolution optical imaging. These galaxies had been classified as double-nucleus galaxies in photographic surveys, but in fact they are normal late-type galaxies. Both galaxies exhibit slowly rising rotation curves characteristic of extremely late type systems, yet with a small bulge component. Analytical models for the potential were applied to describe the mass distribution. A spherical bulge and a disk sufficed to reproduce the main observable properties.

The putative secondary nuclei properties were analyzed, and it was found that they have physical attributes characteristic of giant H II regions: having bluer color indices and being located at the outskirts of the disks, where other similar star-forming regions are also found. They do not seem to be the products of a merger or capture.

The authors wish to thank the staff at BA and CASLEO for assistance, the SOAR staff for carrying out the observations and pre-reducing the data, G. Gunthartd for useful discussions, and the anonymous referee whose useful suggestions helped to improve the manuscript. One of us (G. G.) acknowledges support from a CONICET fellowship. The BA telescope is operated by the Observatorio Astonómico of the Universidad Nacional de Córdoba, Argentina. The CCD and data acquisition system at CASLEO have been partly financed by R. M. Rich through US NSF grant AST 90-15827. The SOAR telescope is operated by the Association of Universities for Research in Astronomy, Inc., under a cooperative agreement between the CNPq, Brazil, and the National Observatory for Optical Astronomy, University of North Carolina, and Michigan State University, USA.

REFERENCES

Boulesteix, J. 1993, ADHOC Reference Manual (Marseilles: Publ. Obs. Marseille)
Dehnen, W. 1993, MNRAS, 265, 250
Díaz, R., Carranza, G., Dottori, H., & Goldes, G. 1999, ApJ, 512, 623
Díaz, R., Dottori, H., Aguero, M., Mediavilla, E., Rodrigues, I., & Mast, D. 2006, ApJ, 652, 1122
Díaz, R., Rodrigues, I., Dottori, H., & Carranza, G. 2000, AJ, 119, 111
Dinerstein, H. 1990, in The Interstellar Medium in Galaxies, ed. H. Thronson & J. Shull (Dordrecht: Kluwer), 257
Gimeno, G., Campos, J. M., Díaz, R., & Calderón, J. 2005a, Bull. Asoc. Argentina Astron., 48, 454
Gimeno, G., Díaz, R., & Carranza, G. 1998, Bull. Asoc. Argentina Astron., 42, 58
———. 1999, Bull. Asoc. Argentina Astron., 43, 67
———. 2000, Bull. Asoc. Argentina Astron., 44, 86
———. 2004, AJ, 128, 62 (Paper I)
———. 2005b, Bull. Asoc. Argentina Astron., 48, 445
Holmberg, E. 1958, Lund. Medd. Astron. Obs. Ser. II, 136, 1
Ibata, R. 2002, in ASP Conf. Ser. 275, Disks of Galaxies, ed. E. Athanassoula, A. Bosma, & R. Mujica (San Francisco: ASP), 141
Joseph, D., Wright, G., James, P., & McLean, I. 1988, MNRAS, 232, 7
Keel, W. 1996, AJ, 111, 696
Lauberts, A. 1982, The ESO/Uppsala Survey of the ESO (B) Atlas (München: ESO)
Leitherer, C., et al. 1999, ApJS, 123, 3
Matthews, L., & Gallagher, J. 2002, ApJS, 141, 429 (MG02)
Mazzarella, J., & Boroson, T. 1993, ApJS, 85, 27
McCall, M., Rybsky, P., & Shields, G. 1985, ApJS, 57, 1
Osterbrock, D. E. 1989, Astrophysics of Gaseous Nebulae and Active Galactic Nuclei (Mill Valley: University Science Books)
Pastoriza, M., Dottori, H., Terlevich, E., Terlevich, R., & Díaz, A. 1993, MNRAS, 260, 177
Satoh, C. 1980, PASJ, 32, 41
Schlegel, D., Finkbeiner, D., & Davis, M. 1998, ApJ, 500, 525
Schweizer, F. 1979, ApJ, 233, 23
Stanghellini, L., & Kaler, J. 1989, ApJ, 343, 811
Vorontsov-Vel'yaminov, B., & Arhipova, V. 1968, Morphological Catalogue of Galaxies, Vol. 4 (Moscow: Moscow Univ.)
Zaritsky, D., & Rix, H.-W. 1997, ApJ, 477, 118